Supporting information

Atomically dispersed Mn within carbon frameworks as high-performance oxygen reduction electrocatalysts for zinc-air battery

Authors: Zhiyu Lin[1], Hao Huang[1], Ling Cheng[1], Yang Yang[1], Ruirui Zhang[1], Qianwang Chen[1, 2*]

Affiliations:

[1]Hefei National Laboratory for Physical Science at Microscale, Department of Materials Science & Engineering, and Collaborative Innovation Center of Suzhou Nano Science and Technology, University of Science and Technology of China, No. 96 JinZhai Road, Hefei 230026, China.

[2]The Anhui Key Laboratory of Condensed Mater Physics at Extreme Conditions, High Magnetic Field Laboratory, Hefei Institutes of Physical Science, Chinese Academy of Sciences, 350 ShuShanHu Road, Hefei 230031, China.

*Correspondence to: cqw@ustc.edu.cn.

Number of pages: 21

Number of figures: 16

Number of tables: 5

1. Material synthesis process
2. Material characterization
3. Electrochemical measurement details
4. Calculation details
5. Supplementary figures and tables

1. Material synthesis process:

Synthesis process of Mn-ZIF: The Mn-containing ZIF-8 MOF precursor (which was denoted as Mn-ZIF) was synthesized as follow: 2 g 2-methylimidazole was dissolved in 20 mL absolute methanol (MeOH) under vigorous stirring to form a clear solution. And then, 0.84 g $Zn(NO_3)_2 \cdot 6H_2O$ was dissolved in 10 mL absolute methanol (MeOH) under ultra-sonication and 138 mg Manganese acetate tetrahydrate ($C_4H_6MnO_4 \cdot 4H_2O$) was dissolved in 10 mL distilled water (H_2O), respectively. Later, the $Zn(NO_3)_2$ solution was first slowly added into above 2-methylimidazole solution under vigorous stirring. Finally, the Manganese acetate tetrahydrate

($C_4H_6MnO_4 \cdot 4H_2O$) solution was added into the mixed solution of 2-methylimidazole and $Zn(NO_3)_2$ as soon as white precipitate was formed in mixed solution. After 1h vigorous stirring, the mixed solution was placed on the experimental bench without any interference for 24 hours until precipitation finished. The precipitation was retrieved by centrifugation and washed with methanol for several times to remove the reaction residue. The precipitation (Mn-ZIF) was then dried in vacuum oven.

Synthesis of Mn-SA catalyst: To obtain the Mn-SA catalyst, the Mn-ZIF was directly carbonized in a nitrogen flow under 900 ℃ with a heating rate of 5 ℃ min^{-1} and kept at 900 ℃ for 3 hours in the carbonized process.

Synthesis process of the zeolitic imidazolate framework (ZIF-8): The whole synthesized route of zeolitic imidazolate framework (ZIF-8) was similar to Mn-ZIF above except that there was no Manganese acetate tetrahydrate was added. ZIF-8 was synthesized as follow: 2 g 2-methylimidazole was dissolved in 20 mL absolute methanol (MeOH) under vigorous stirring to form a clear solution and 0.84 g $Zn(NO_3)_2 \cdot 6H_2O$ was dissolved in 10 mL absolute methanol (MeOH) under ultra-sonication, respectively. Then, the $Zn(NO_3)_2$ solution was slowly added into above 2-methylimidazole solution under vigorous stirring and keep stirring for an hour. The mixed solution was placed on the experimental bench without any interference for 24 hours until precipitation finished. The precipitation was retrieved by centrifugation and washed with methanol for several times to remove the reaction residue. The precipitation (ZIF-8) was then dried in vacuum oven.

Synthesis of N/C: To obtain N/C material, the ZIF-8 MOF precursor was directly carbonized in a nitrogen flow under 900 ℃ with a heating rate of 5 ℃ min^{-1} and kept at 900 ℃ for 3 hours in the carbonized process.

Synthesis of S-1, S-2 and S-3: To study the optimization of Mn concentration for precursor synthesis, a series of samples were synthesized through changing the usage of manganese acetate tetrahydrate. Instead of 138mg, the usage of manganese acetate tetrahydrate were 69mg, 207mg and 276mg, respectively. Other reaction conditions are consistent with those of Mn-SA. The corresponding final catalysts were named S-1, S-2 and S-3.

2. Material characterization:

The powder XRD patterns were acquired by an X-ray diffractometer (Japan Rigaku D/MAX-γA) with Cu Kα radiation (λ=1.54178 Å). FESEM images were filmed on a JEOLJSM-6700 M scanning electron microscope. TEM images were taken on a Hitachi H-800 transmission electron microscope using an accelerating voltage of 200 kV, and a HRTEM (JEOL-2011) was operated at an accelerating voltage of 200 kV. The high-angle annular dark-field scanning transmission electron microscopy (HAADF-STEM) and corresponding energy-dispersive spectroscopy (EDS) mapping analyses were carried out on a JEOL JEM-ARF200F TEM/STEM with a spherical aberration corrector. Raman spectra were obtained through a LabRAM HR Raman spectrometer and Fourier transform infrared (FT-IR) spectra were measured by a Magna-IR 750 spectrometer. XPS measurements were executed on an ESCALAB 250 X-ray photoelectron spectrometer using Al Kα radiation. Inductively coupled plasma atomic emission spectroscopy (ICP-AES) result was measured by using an Optima 7300

DV instrument. The sample towards ICP analysis was first heated at 900 ℃ and kept at the temperature for 5 h in air which was followed by treatment in concentrated chloroazotic acid for a few minutes under ultra-sonication until the residue was fully dissolved. The X-ray absorption near edge structure (XANES) of C K-edge, N K-edge were measured at the soft X-ray magnetic circular dichroism end station (XMCD) of National Synchrotron Radiation Laboratory (NSRL) in University of Science and Technology of China (USTC). The X-ray absorption near edge structure (XANES) and the extended X-ray absorption fine structure (EXAFS) of Mn were investigated at BL14W1 beamlines of Shanghai Synchrotron Radiation Facility (SSRF). The Mn-SA catalyst were characterized using Mn K-edge XANES and EXAFS in a fluorescence mode. The Mn-foil and the samples used as reference were characterized in a transmission mode. The absorption spectra of Mn K-edge for all samples were acquired using a Si (111) double-crystal monochromator at BL14W1 beamline. The obtained data was normalized and analyzed by Athena software. The background subtraction and normalization procedures were performed using standard routines with default parameters determined by Athena software. The fitting of the EXAFS spectra was carried out using Artemis software.

3. Electrochemical measurement details:

All of the electrochemical tests were carried out using a three-eletrode system on an electrochemical workstation (CHI760E). A glassy carbon (GC) electrode (diameter of 5 mm with surface area of 0.196 cm^2) was used as a working electrode, while graphite rod was utilized as the counter electrode. The potential was recorded using Ag/AgCl (3.5 M KCl) electrode as the reference electrode. All of

the potentials were calibrated to the reversible hydrogen electrode (RHE) according to Nernst equation. Typically, to prepare the working electrode in this article, 4 mg of the catalysts and 30 μL Nafion solution (Sigma Aldrich, 5 wt.%) were dispersed in 1 mL ethanol solution and sonicated for1 h to form a homogeneous ink. And then, 10 μL of the dispersion was slowly loaded onto the glassy carbon electrode (catalyst loading 0.2 mg/cm^2). Before the ORR catalytic activity measurement, oxygen was used to purge the 0.1 M KOH solution for 30 min to guarantee the solution oxygen saturation. The working electrodes were active using CV test with a scan rate of 100 mVs^{-1} for several segments before cyclic voltammetry (CV) and Linear sweep voltammetry (LSV) tests. And the polarization curves of the ORR was measured from 0.2 to 1.1 V (V vs RHE) at a scan rate of 10 mV s^{-1} with a series of rotating electrode speeds using a MSR Electrode Rotator (Pine Research Instrumentation). As a common reference in ORR catalytic test, 20 wt% Pt/C catalyst was measured with the same loading amount. To deduct the contribution of electrochemical double-layer capacitance (Cdl) to the ORR current density, the ORR current was calculated by deducting the current measured in N_2-saturated electrolyte (0.1M KOH) from the current measured in the O_2-saturated electrolyte (0.1M KOH).

The RDE tests were measured at various rotating speed from 400 to 2025 rpm with a sweep rate of 10 mV· s^{-1}. The electron transfer number (n) was calculated by the slopes of their Koutecky‑Levich (K-L) plots' (J^{-1} vs. $w^{-1/2}$) linear fit lines from the K-L equation:

$$1/J = 1/J_K + 1/J_L = 1/J_K + 1/Bw^{1/2} \quad (S1)$$

$$B = 0.62nFC_0D_0^{2/3}V^{-1/6} \quad (S2)$$

where J is the measured current density, J_K and J_L are the kinetic-and diffusion limiting current densities, w is the angular velocity, n is transferred electron number, F is the Faraday constant (96485 C mol^{-1}), D_0 is the diffusion coefficient of O_2 ($1.9\times10^{-5}cm^2\ s^{-1}$), C_0 is the bulk concentration of O_2 (1.2×10^{-6} mol cm^{-3}), V is the kinematic viscosity of the electrolyte (0.01 $cm^2\ s^{-1}$), and k is the electron-transfer rate constant.

The detail of RRDE measurement: Rotating ring-disk electrode (RRDE) test was performed on a RRDE configuration (Pine Research Instrumentation) with a disk electrode ((glassy carbon, area: 0.2475 cm^2) and a ring electrode (Pt electrode, area 0.1866 cm^2). The measurement was performed at a constant ring potential of 1.3 V versus RHE.

The electron transfer number (n) and the peroxide yield (H_2O_2%) were calculated using following equations according to the reference 1:

$$n=4\frac{i_d}{i_d+i_r/N} \qquad (S3)$$

$$H_2O_2(\%)=200\frac{i_r/N}{i_d+i_r/N} \qquad (S4)$$

where i_d and i_r are disk and ring current densities, respectively. N is the current collection efficiency of the Pt ring which is 0.37.

Zinc-air battery tests: A polished zinc plate was served as the anode (surface area: 1.69 cm^2) and the carbon paper (HCP030) which was coated with Mn-SA catalyst ink (cathode area: 1 cm^2; catalyst loading: 2mg/cm^2) was used as cathode in the home-made zinc-air battery device. The current density for assessing the performance of the Zn-air battery is calculated by using the surface area of cathode. The electrolyte used in the zinc-air battery was 6 M KOH. The 20% Pt/C catalyst

was also prepared with the same procedure and loading amount and its performance was tested for comparison.

4. Calculation details：

We performed the DFT calculation using the Vienna Ab Initio Simulation Package (VASP). This code solves the Kohn-Sham equations of density functional theory (DFT) using a plane-wave basis set and the projector augmented wave (PAW) method. The generalized gradient approximation (GGA) of Perdew−Becke−Ernzerhof (PBE) is used for the exchange-correlation functional. The cut-off energies for plane waves is 400 eV. And all structures were optimized with a convergence criterion of 1×10^{-5} eV for the energy and 0.02 eV/Å for the forces. A Monkhorst-Pack $3\times3\times1$ k-point grid was used to sample the Brillouin zone for structure optimization and $7\times7\times1$ k-point grid was used for DOS calculation. The free energies of the intermediates at 298.15 K were obtained using following equation according to previous work:

$$\Delta G=\Delta E+\Delta ZPE-T\Delta S+eU \qquad (S5)$$

where ΔE is the binding energy of adsorption species OH*, O* and OOH*, ΔZPE, ΔS and U are the zero point energy changes, entropy changes and applied potentials, respectively.

5. Supplementary figures and Tables

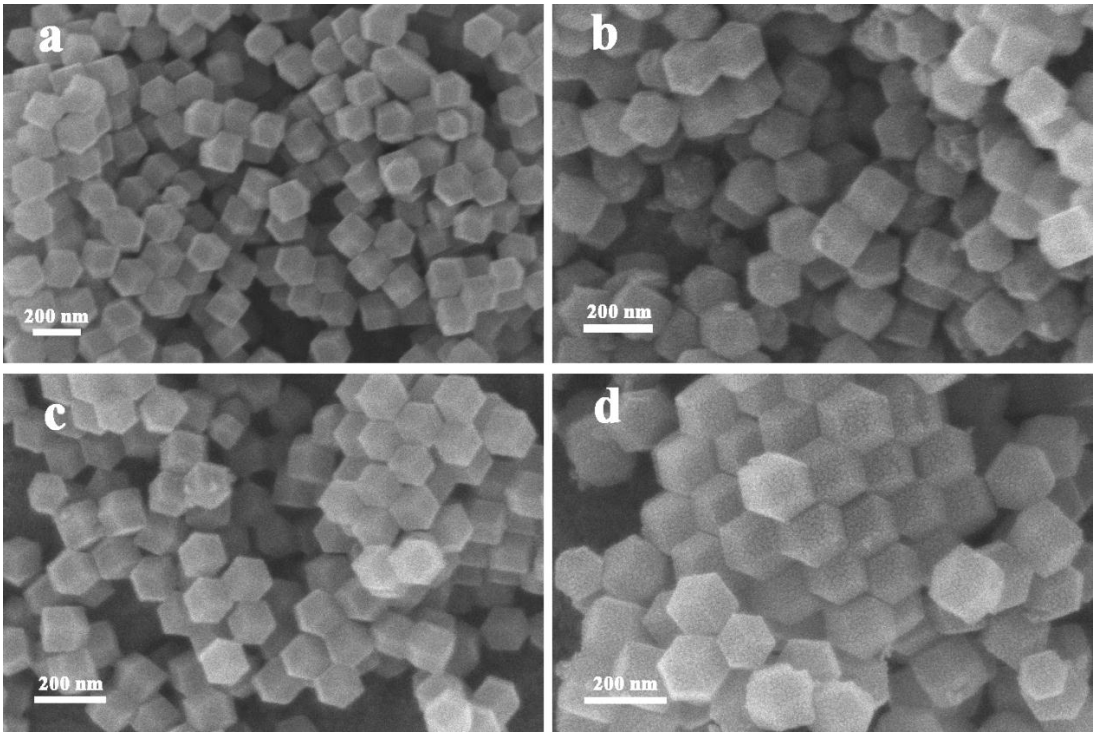

Figure S1. The FESEM characterization of ZIF-8, N/C, M-ZIF and Mn-SA catalyst. The FESEM images of ZIF-8 (a), N/C (b), M-ZIF (c) and Mn-SA catalyst (d).

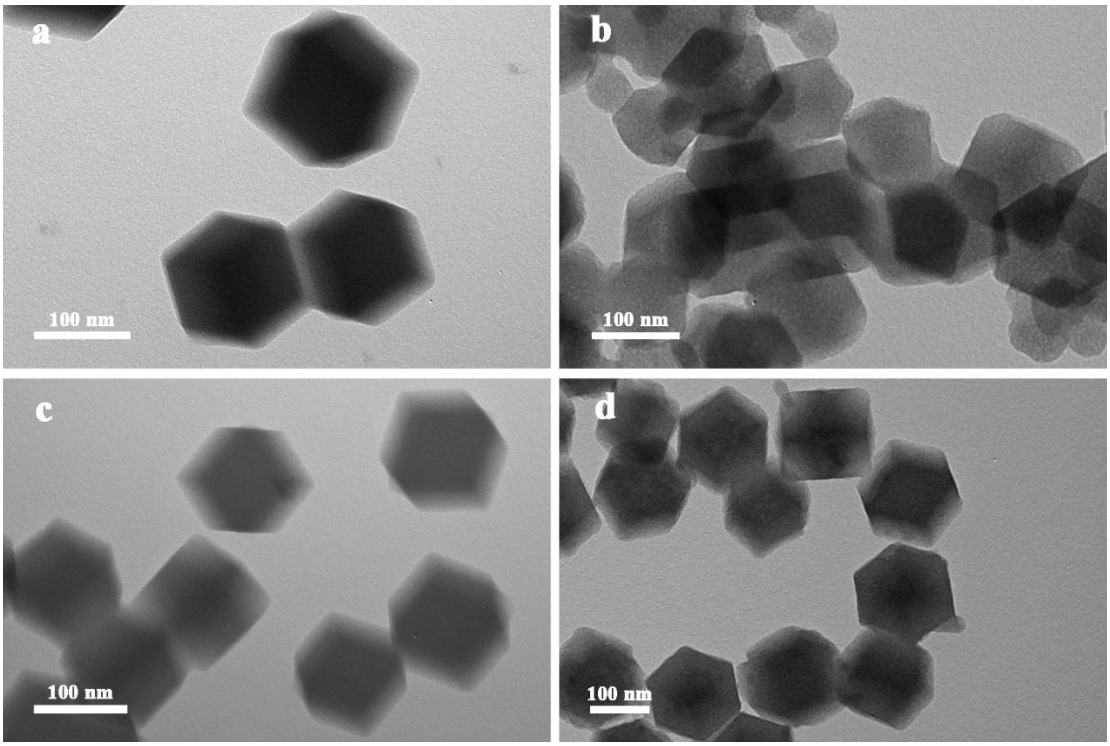

Figure S2. The TEM characterization of ZIF-8, N/C, M-ZIF and Mn-SA catalyst. The TEM images of ZIF-8 (a), N/C (b), M-ZIF (c) and Mn-SA catalyst (d).

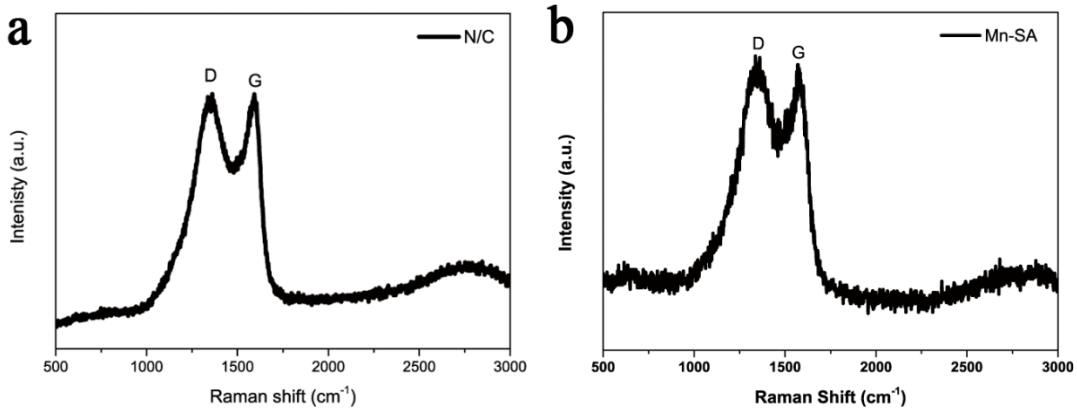

Figure S3. Raman spectrum of N/C (a) and Mn-SA (b).

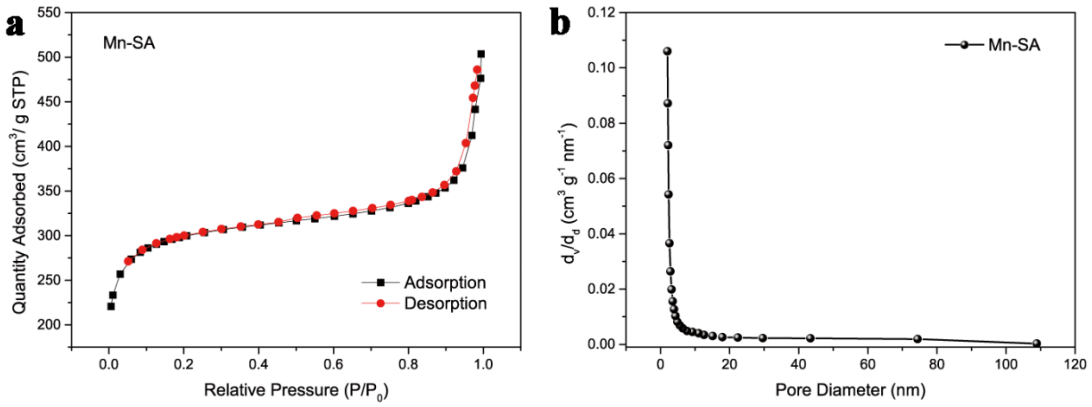

Figure S4. (a) Nitrogen adsorption and desorption isotherm curves of Mn-SA material. (b) Pore size distribution curve of Mn-SA material.

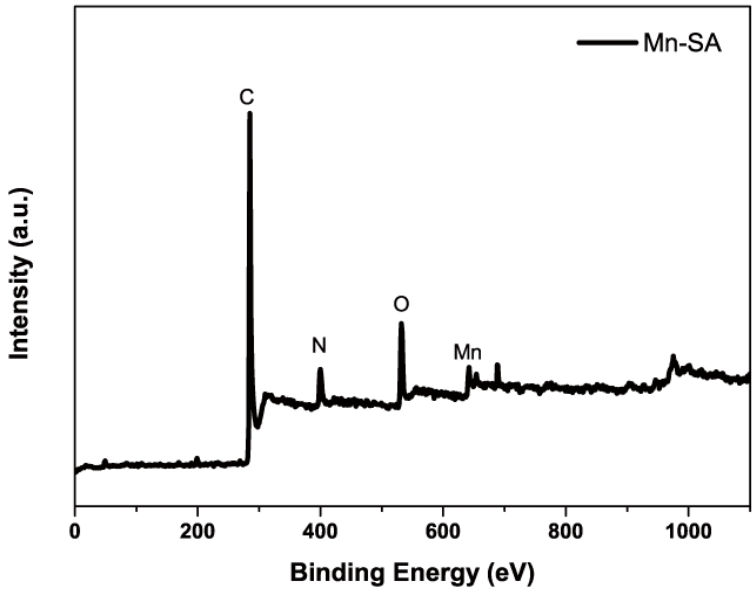

Figure S5. The XPS survey spectrum of Mn-SA.

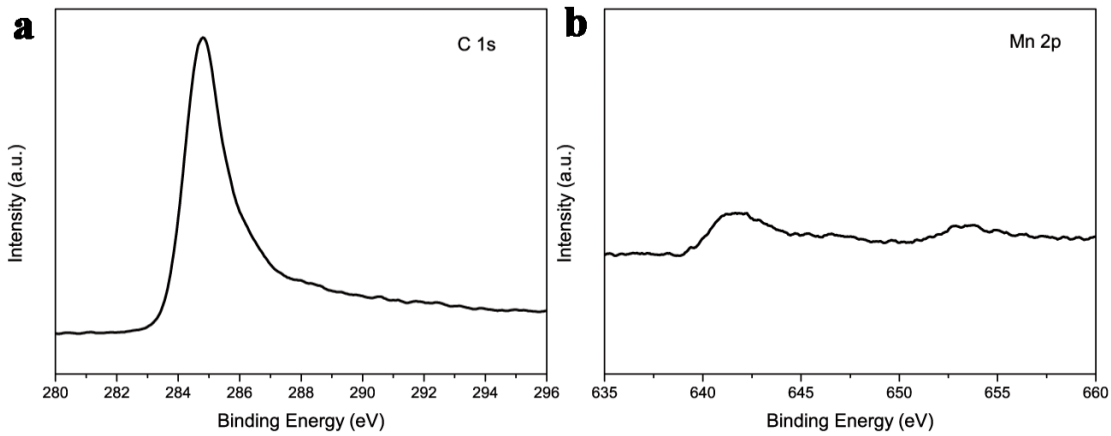

Figure S6. XPS spectra of Mn-SA. (a) C 1s spectrum. (b) Mn 2p spectrum.

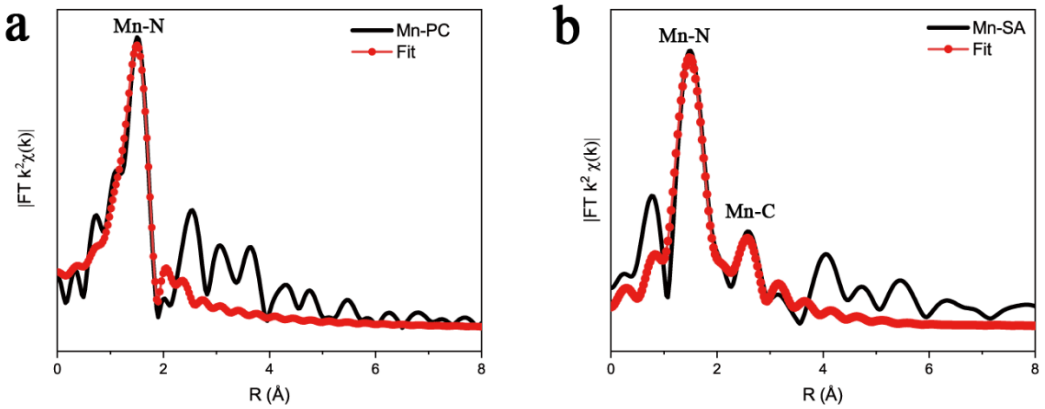

Figure S7. The fitting curves in R space of Mn-PC (a) and Mn-SA (b).

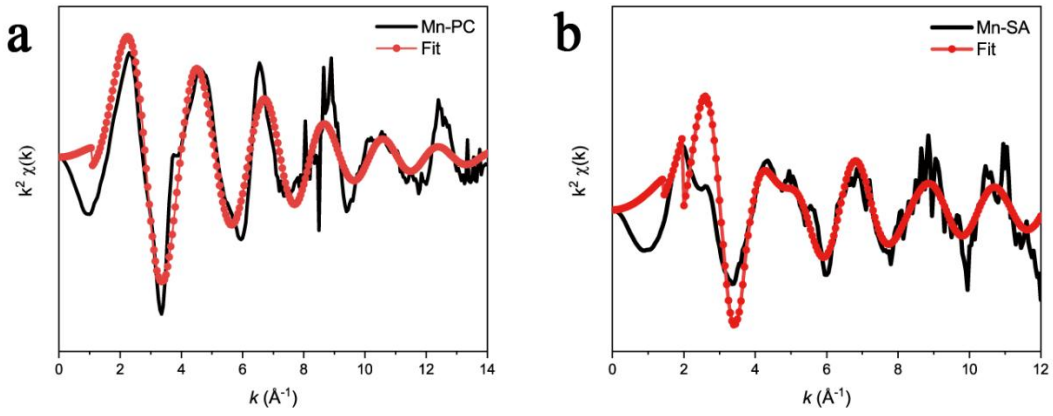

Figure S8. The fitting curves in k space of Mn-PC (a) and Mn-SA (b).

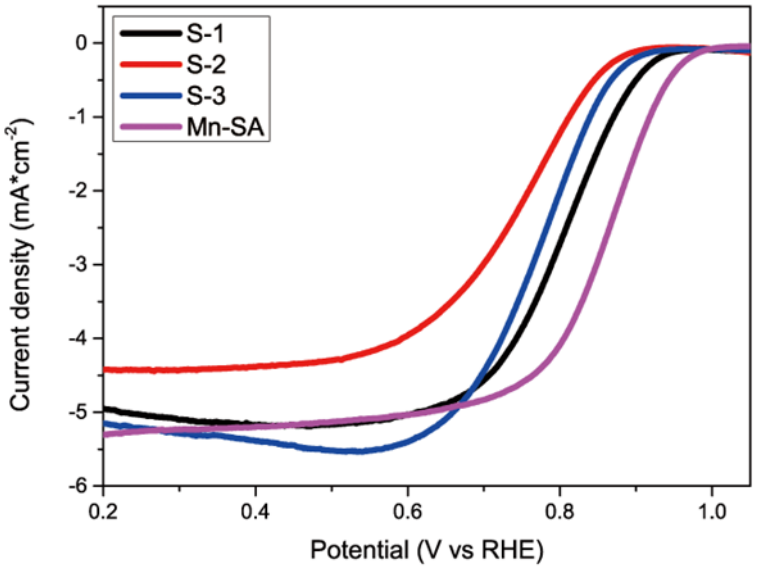

Figure S9. The ORR performance tests of different samples to study the optimization of Mn concentration for precursor synthesis.

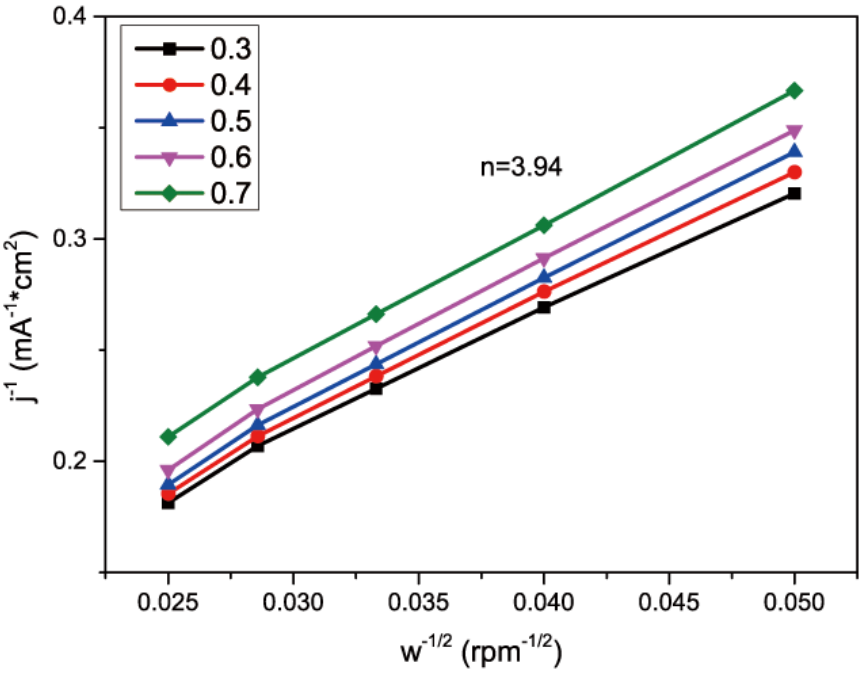

Figure S10. K-L plots of Mn-SA catalyst at different potentials.

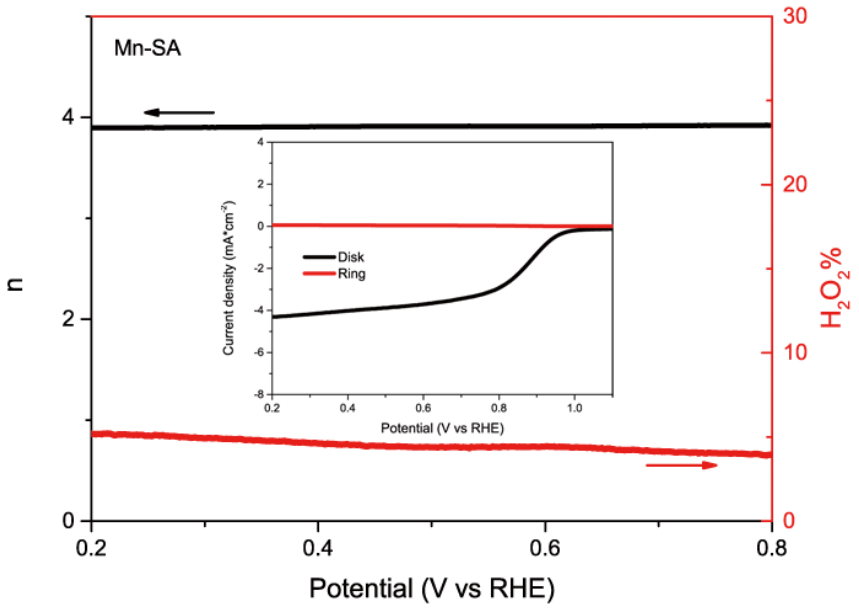

Figure S11. H_2O_2 yield for oxygen reduction reaction and the number of transfer electrons (n) measured by the RRDE method (the inset in Figure S8 presents the RRDE voltammograms).

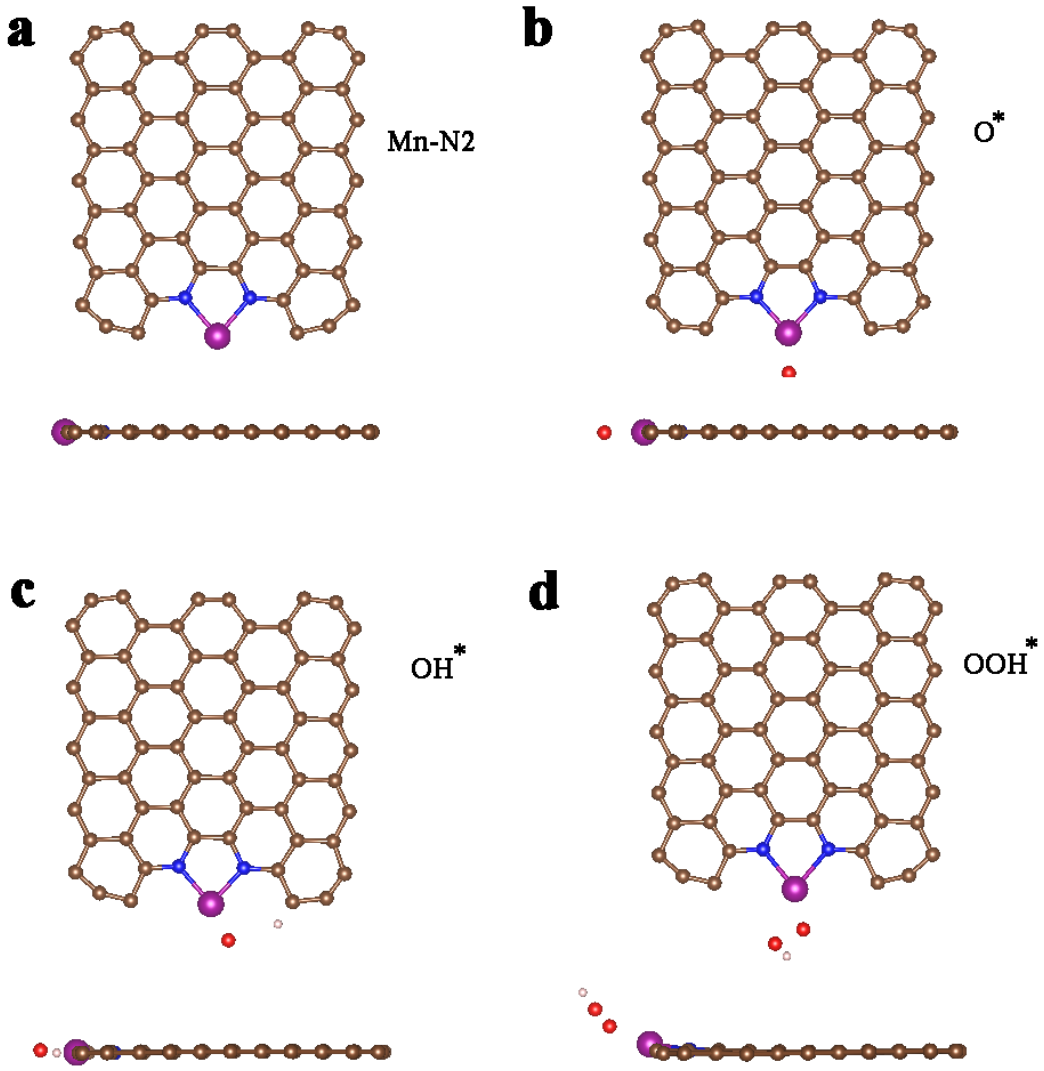

Figure S12. The optimized Mn-N_2 model (a) and Mn-N_2 surface with different ORR intermediate O* (b), OH* (c) and OOH* (d). Brown, blue, violet, red and white balls represent C, N, Mn, O and H atoms, respectively. Each model is illustrated from both top view and side view.

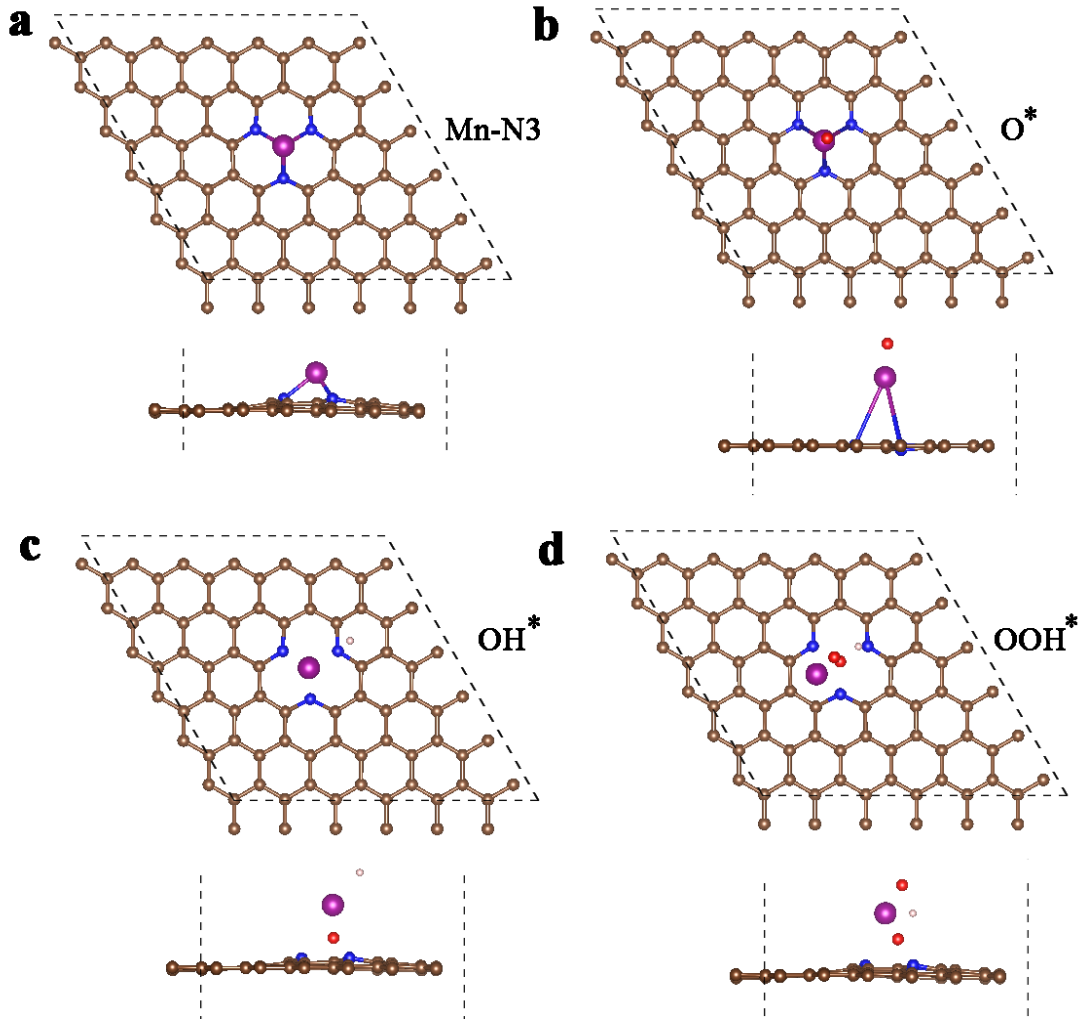

Figure S13. The optimized Mn-N_3 model (a) and Mn-N_3 surface with different ORR intermediate O* (b), OH* (c) and OOH* (d). Brown, blue, violet, red and white balls represent C, N, Mn, O and H atoms, respectively. Each model is illustrated from both top view and side view.

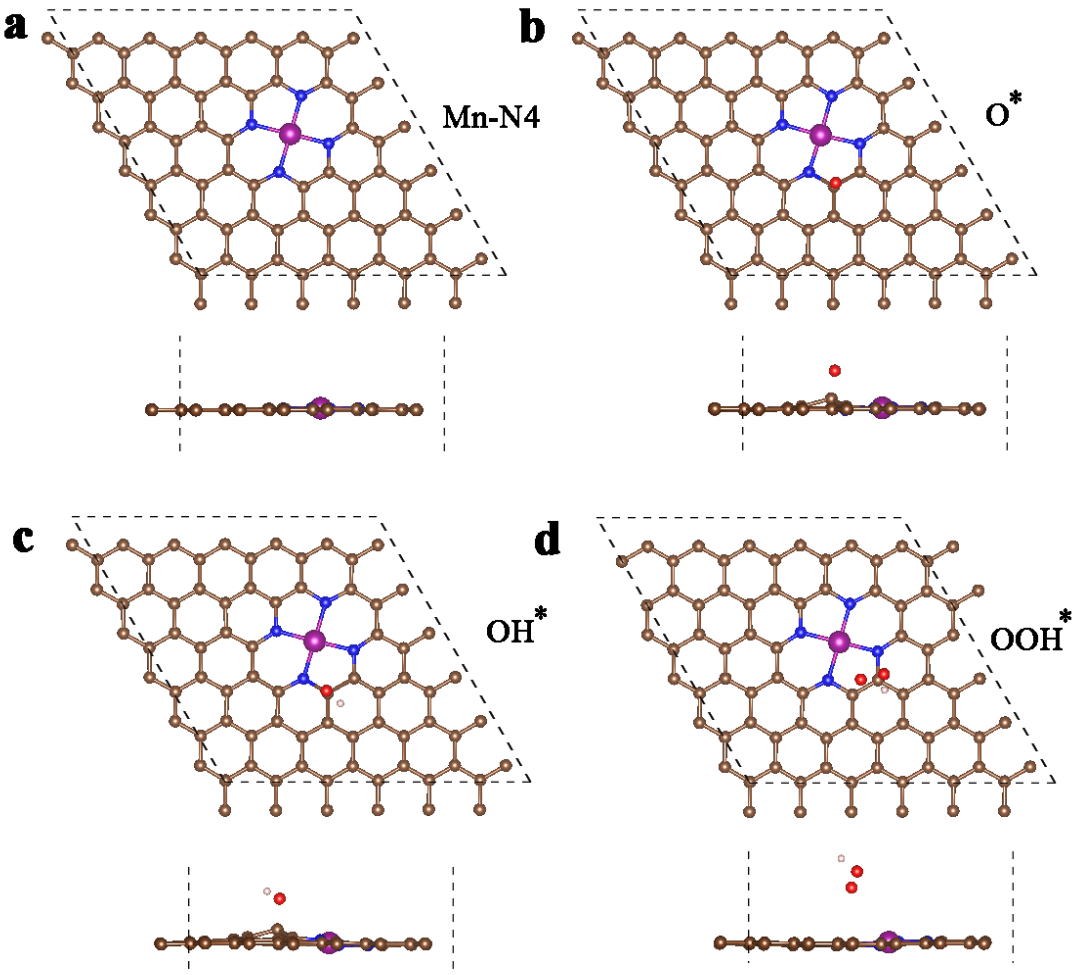

Figure S14. The optimized Mn-N_4-C model (a) and Mn-N_4-C surface with different ORR intermediate O* (b), OH* (c) and OOH* (d). Brown, blue, violet, red and white balls represent C, N, Mn, O and H atoms, respectively. Each model is illustrated from both top view and side view. (NOTE: the adsorption site of ORR intermediates is the carbon atom near the Mn-N_4 configuration, which is different from that of in the manuscript.)

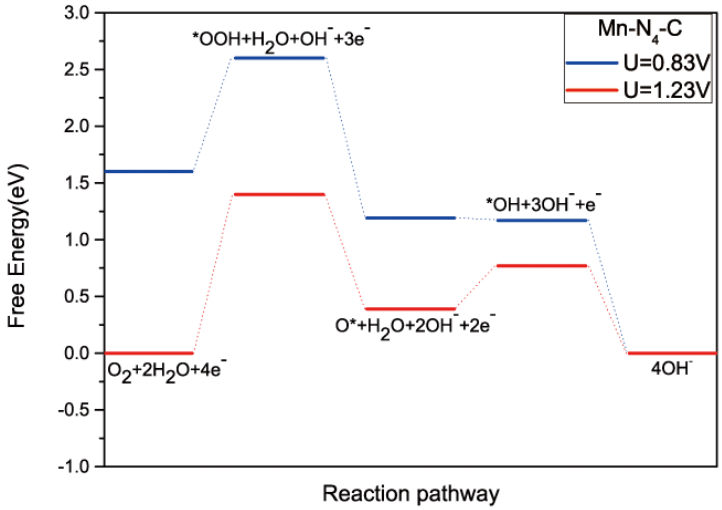

Figure S15. Free energy diagram of ORR on Mn-N_4-C surface under different overpotentials. (NOTE: the adsorption site of ORR intermediates is the carbon atom near the Mn-N_4 configuration, which is different from that of in the manuscript.)

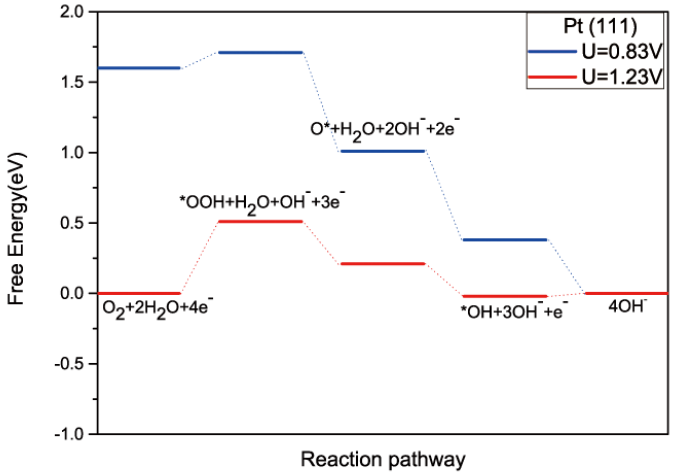

Figure S16. Free energy diagram of ORR on Pt (111) surface under different overpotentials.

Table S1. Summary of the specific surface area, pore volume and pore diameter of Mn-SA catalyst.

Sample	**BET surface (m^2/g)**	**Total pore volume (cm^3/g)**	**Pore diameter (nm)**
Mn-SA	1014.2	0.35	8.5

Table S2. Chemical compositions of prepared samples determined by XPS measurement.

Samples	C(atom%)	N(atom%)	Mn(atom%)	O(atom%)
Mn-SA catalyst	81.74	7.66	1.27	9.33

Table S3. EXAFS data fitting results of different samples.

Sample	Path	N	R(Å)	σ2($Å^2$)	ΔE_0(eV)
Mn-PC	Mn-N	3.5±0.4	1.97±0.02	0.005	4.5
Mn-SA	Mn-N	3.2±0.8	1.96±0.04	0.001	7.5
	Mn-C	5.4±10	2.89±0.16	0.01	15

Notes: N is the coordination number; R represents the distance between absorber and backscatter atoms; σ2 is the Debye-Waller factor value; ΔE_0 is the inner potential correction to account for the difference in the inner potential between the sample and the reference compound.

Table S4. Comparison of the ORR activity between Mn-SA and other Mn-based catalyst and metal-single-atoms ORR catalysts in alkaline conditions (0.1M KOH) documented in the literature.

Catalysts	loading (mg*cm-2)	Onset potential (V vs RHE)	Half-wave potential (V vs RHE)	Reference
Mn-SA	**0.2**	**0.99**	**0.87**	**This work**
D-AC@2Mn-4Co	0.16	0.88	0.8	Adv. Mater. 2016, 28, 8771–8778
Mn_3O_4-CoO/CNT	0.4	0.84	0.75	J. Mater. Chem. A,2014,2,3794

Mn_3O_4/Mxene	0.1	0.89	not given	J. Mater. Chem. A, 2017, 5, 20818
Mn_xO_y-NC	0.21	not given	0.81	Angew Chem Int Edit 2014, 53, 8508.
$MnO_{1.74}$	0.12	0.93	0.73	Chem. Commun., 2015, 51, 11599
$MnCo_2O_4$	0.2	0.95	0.83	Angew. Chem. 2017, 129, 15173
Fe-N-CNFs	0.6	0.93	0.82	Angew. Chem. Int. Ed. 2015, 54, 8179-8183.
Co SAs/N-C(900)	0.41	not given	0.88	Angew Chem Int Edit 2016, 55, 10800.

Table S5. Calculated d-band center position relative to Fermi level for various Mn based models.

Optimized structure	d-band center position
Mn-N2	-3.29eV
Mn-N3	-3.26eV
Mn-N4	-3.17eV

Reference:

1. Sultan, S.; Tiwari, J. N.; Jang, J. H.; Harzandi, A. M.; Salehnia, F.; Yoo, S. J.; Kim, K. S. Highly Efficient Oxygen Reduction Reaction Activity of Graphitic Tube Encapsulating Nitrided CoxFe gamma Alloy. Adv Energy Mater 2018, 8, 1801002.